metals

MDPI

Article

Effective and Environmentally Friendly Nickel Coating on the Magnesium Alloy

Ivana Škugor Rončević *, Marijo Buzuk and Nives Vladislavić

Department of General and Inorganic Chemistry, Faculty of Chemistry and Technology, University of Split, R. Boškovića 35, 21000 Split, Croatia; buzuk@ktf-split.hr (M.B.); nives@ktf-split.hr (N.V.)

* Correspondence: skugor@ktf-split.hr; Tel.: +385-213-29472

Academic Editor: Hugo F. Lopez

Received: 19 October 2016; Accepted: 2 December 2016; Published: 10 December 2016

Abstract: The low density and good mechanical properties make magnesium and its alloys attractive construction materials in the electronics, automotive, and aerospace industry, together with application in medicine due to their biocompatibility. Magnesium AZ91D alloy is an alloy with a high content of aluminum, whose mechanical properties overshadow the low corrosion resistance caused by the composition of the alloy and the existence of two phases: α magnesium matrix and β magnesium aluminum intermetallic compound. To improve the corrosion resistance, it is necessary to find an effective protection method for the alloy surface. Knowing and predicting electrochemical processes is an essential for the design and optimization of protective coatings on magnesium and its alloys. In this work, the formations of nickel protective coatings on the magnesium AZ91D alloy surface by electrodeposition and chemical deposition, are presented. For this purpose, environmentally friendly electrolytes were used. The corrosion resistance of the protected alloy was determined in chloride medium using appropriate electrochemical techniques. Characterization of the surface was performed with highly sophisticated surface-analytical methods.

Keywords: chemical deposition; magnesium alloy; nickel; self-assembling monolayer; surface modification

1. Introduction

Magnesium and its alloys are construction materials exhibiting a high strength and low density, together with high-temperature and low electromagnetic conductivity. Easy machine processing and recycling enables the use of magnesium for the production of a car parts, computers, mobile phones, hand tools, and so forth. A low resistance to corrosion, abrasion, and creep, as well as high chemical reactivity, limits its practical application. One of the most effective ways to improve the poor corrosion resistance of magnesium and its alloys is the formation of a protective coating on its surface, which protects the underlying material from the aggressive media [1]. In order to ensure adequate corrosion protection, coating must be uniform, well-tied to the matrix, pore-free, and self-renewable at sites on which its physical destruction can be expected. Various techniques have been developed for applying a protective coating to the surface, such as: electrochemical deposition, chemical deposition, conversion coating, anodizing, organic coating, and deposition processes from the vapor phase [2]. Electrodeposition and chemical deposition enable the easy formation of corrosion-resistant film on the magnesium alloy surface [3,4] by reduction of the metal cations in the solutions of metal ions. However, two main reasons are responsible for difficulties encountered as a result of both kinds of deposition on magnesium alloys [5,6]. The first one is the microstructure of the magnesium AZ91D alloy, as it is composed of an α phase matrix and β phase (intermetallic compound $Mg_{17}Al_{12}$) [7] with different electrochemical properties. The electrode potential of the α phase is −1.00 V and the electrode potential of the β phase is −1.73 V. As a result, the alloy is heterogeneous, which can cause galvanic corrosion. Accordingly, achieving a high-quality coating on magnesium alloys

with conventional methods is difficult or even impossible since the corrosion of the substrate and plating are two simultaneous competitive reactions [4]. This can be overcome by applying various pretreatment procedures for each type of magnesium alloy [8], thus obtaining a heterogeneous surface suitable for further coating. For example, Yang et al. modified the surface of the AZ91D alloy by chemical pretreatment. The process included alkaline conditioning and acid activation in different nontoxic (fluoride-free) acid solutions. As a result of this pretreatment, effective dissolving of the β phase from the AZ91D alloy surface was obtained. Furthermore, this surface pretreatment optimized the subsequent coating and allowed tuning of the anodic and cathodic activity on the surface by allowing one to control the Mg/Al molar ratio. [9]. As the magnesium alloy has an electrode potential lower than electrode potential of structural metals, each metal layer on the magnesium alloy acts as a cathode coating. Therefore, films obtained by electrodeposition or chemical deposition must be highly compact. Otherwise, effective protection will not be achieved, but will accelerate corrosion of the substrate [4]. The second difficulty is the extremely high chemical reactivity of magnesium and magnesium alloys, which results in formation of a nonuniform oxide or hydroxide film at the alloy surface. This layer has a negative effect on the adhesion and uniformity of the coating. Different approaches for obtaining a homogenous layer (on magnesium alloy) suitable for further coating (such as nickel) have been reported. Considerable literature is available on corrosion-resistant coatings for magnesium and its alloys, and Chen et al. have published an excellent review article of conversion coatings for magnesium by coating type and by pretreatment process [10]. However, some of methods include harmful chemicals such as chromate [2], fluoride [11], and vanadium [12], which is contrary to the environmental protection regulative [13]. In addition, conversion coatings based on stanate [14,15], rare elements [16], and ionic liquids [17], at this point, are not applicable for practical use. Also, a pretreatment including phosphate/phosphate-manganate [18], molten salt [19], and stearic acid [20] were reported. The growing concern for environmental protection has led to setting up more stringent regulations regarding the use of chemicals that may have a harmful effect on the environment, which has led to a reduction or complete termination of the use of a number of very effective conversion coatings. Also, the use of polyphosphates was reduced, because it was found that their release into the natural waterways can lead to excessive eutrophication. Additionally, due to toxicity, the use of amine, arsenic oxide, and propargyl alcohol in preparation of conversion coatings is limited [21]. Therefore, this problems leads to the concept of formation environmentally friendly pretreatment layer, after homogeneous film of nickel can be obtained. Surface-coating techniques for magnesium alloys that have been commercially used are: (i) immersion in a solution of zincate or copper ions; (ii) a prior chemical deposition followed by plating nickel directly; and (iii) formation of a pretreatment layer using environmentally friendly compounds [2]. Acid etching, alkaline etching, and activation in chemical deposition and electrodeposition methods have a large influence on the adhesion of deposits to the substrate surface [4]. Currently, the magnesium alloys are etched in a solution of chromium oxide and nitric acid, and soaked in a hydrofluoric acid (HF) solution. Although the chromate effectively reduces corrosion, it is toxic and potentially cancerous [22]. Therefore, the tendency in the industry is to eliminate hexavalent chromium from the pretreatment procedures and replacement it with nontoxic and environmentally friendly compounds [8]. An environmentally friendly chemical deposition process is considered to be the one in which hydrofluoric acid is not used (or only a small amount is used) and chromate is replaced by stannates [15,23], phosphates permanganate [22,24], or molybdates [25].

In this paper, we describe the alkylphosphonic acid pretreatment coating (which is also referred to as conversion coating), followed by nickel chemical deposition onto the AZ91D Mg alloy substrate. The alkylphosphonic acid pretreatment coating should be sealed with an alcoholic solution of γ-aminopropyltriethoxysilane (APTES) to reduce the possibility of galvanic corrosion caused by cracking of the porous layer [8].

In this work, a nickel protective coating was formed by chemical and electrochemical deposition. Studies were conducted to characterize the electrochemical behavior of the unmodified and modified

magnesium AZ91D alloy samples in the chloride electrolyte solutions using electrochemical impedance spectroscopy (EIS) and voltammetry methods, while for the microstructure characterization of the films, analytical surface methods (X-ray photoelectron spectroscopy (XPS), Fourier-transform infrared spectroscopy (FTIR), etc.) were used.

2. Experimental Section

Electrochemical studies of unmodified and modified AZ91D magnesium alloy samples were carried out in chloride electrolyte solution in a standard electrochemical reactor with a platinum counter electrode and reference Ag/AgCl/3 M KCl electrode (Metrohm, Herisau, Switzerland), whose potential is +0.209 V with respect to the standard hydrogen electrode. All measured values of the electrochemical potential in this paper are compared to the potential of the reference electrode. Before each modification of the alloy surface (as pretreatment for the chemical or for the electrochemical deposition of nickel), AZ91D magnesium alloy samples (surface area of 0.235 cm^2) were abraded successively with metallographic abrasive paper gradations of 800, 1000, 1200, and 2000 followed by successively treatments with metallographic abrasive pastes (Buehler MicroPolish Alpha Alumina, Lake Bluff, IL, USA) of fineness 1 μm, 0.3 μm, and 0.05 μm to achieve a mirror finish. After that, the electrode was washed in distilled water and degreased in 96% ethanol in an ultrasonic bath for 3 min. After degreasing, the working electrode was dried under nitrogen. This prepared electrode was then modified by different pretreatments (depending of the nickel deposition method) as follows.

Dodecylphosphonic acid (DDPA) conversion coatings were self-assembled on the surface of AZ91D alloy covered with a natural oxide film (spontaneously passivated) by the immersion of alloy in DDPA alcoholic solution (concentration range from 0.5 $mmol \cdot dm^{-3}$ to 10 $mmol \cdot dm^{-3}$) at room temperature for 1–4 h. Pretreatment coating (DDPA self-assembled monolayer (SAM), $C_{12}H_{27}PO_3$) formed using optimal conditions (concentration of 0.7 mM and time of immersion in the alcoholic solution of 1 h) was then silylated.

For the silylation process, an alcoholic solution of γ-aminopropyltriethoxysilane (APTES—$H_2N(CH_2)_3Si(OC_2H_5)_3$) (10 μL, 1:1) spiked with 0.0088 g of palladium chloride was used. Silylation was performed for 20 min. On the above-prepared electrode surface layer, chemical (electroless) deposition of nickel was performed. For this purpose, we used a bath composition as follows: 35 $g \cdot dm^{-3}$ nickel(II) acetate ($Ni(CH_3COO)_2$), 20 $g \cdot dm^{-3}$ sodium hypophosphite ($NaH_2PO_2 \times H_2O$), 26 $g \cdot dm^{-3}$ 2-hydroxypropanoic acid ($CH_3CHOHCOOH$), 14 $g \cdot dm^{-3}$ hydroxybutanedioic acid ($C_2H_3OH(COOH)_2$), 25 $g \cdot dm^{-3}$ sodium acetate trihydrate ($NaCH_3COO \times 3H_2O$), and 3 $g \cdot dm^{-3}$ ammonium sulfate ($(NH_4)_2SO_4$).

For electrochemical plating of the AZ91D magnesium alloy, samples were mechanically treated (as previously mentioned) followed by alkaline degreasing in a solution of NaOH (60 °C) for 5 min after samples had been degreased in ethanol. Furthermore, samples of alloy were washed with distilled water and dried in a hot air stream.

Activation (etching) was performed for a period of 2 min in a solution of 10% H_2SO_4. On the obtained prepared electrode surface, nickel was electrochemically deposited using Watts plating baths of the following composition: nickel (II) sulfate hexahydrate, nickel (II) chloride hexahydrate, and boric acid (40 °C, pH 4). For this purpose, a nickel anode was used as a counter electrode. Plating was performed at a constant current of −5.88 mA. The applied current produced voltage of around −1.95 V. Electrochemical tests were carried out in a solution with a chloride concentration of 0.174 $mol \cdot dm^{-3}$. Corrosion resistances of unmodified and modified surfaces of the AZ91D magnesium alloy were studied using electrochemical impedance spectroscopy (EIS) (Ametek Solartron Metrology, Leicester, England). Electrochemical impedance spectra were recorded at an open-circuit potential (E_{ocp}) after 30 min of stabilization at the same potential with a frequency ranging from 100 kHz to 0.1 Hz with signal amplitude of 5 mV.

Spectra were fit with a suitable electric equivalent circuit (EEC) using complex nonlinear least squares method (CNLS algorithm); the values of elements of the proposed circle show chi-square values (χ^2) with orders of magnitude of 10^{-3} (errors of 0.5%–3%).

All electrochemical measurements were carried out using the following instruments: (1) potentiostat/galvanostat EG&G Princeton Applied Research (PAR) model 273A (Princeton Applied Research Corporation, Princeton, NY, USA), (2) potentiostat/galvanostat Solartron SI 1287 (Ametek Solartron Metrology, Leicester, England), and (3) high-frequency (HF) frequency response analyzer (FRA) Solartron SI 1255 (Ametek Solartron Metrology, Leicester, England). Solartron instruments are controlled by computer programs ZPlot (Scribner Associates Inc., Southern Pines, NC, USA) and CorrWare (Scribner Associates Inc., Southern Pines, NC, USA). To control the PAR instrument, the ECHEM program (eDAQ, Denistone East, Australia) was used; for the data processing ZView (Scribner Associates Inc., Southern Pines, NC, USA) and CorrView (Scribner Associates Inc., Southern Pines, NC, USA) software were used.

Surface characteristics of AZ91D alloy modified with DDPA SAM were determined by the contact angle, X-ray photoelectron spectroscopy (XPS), and Fourier-transform infrared spectroscopy (FTIR) measurements.

Contact angle measurements were carried out on contact-angling measuring (CAM) device OCA 20 (DataPhysics Instruments GmbH, Filderstadt, Germany) at a constant temperature of 25.0 ± 0.5 °C, and the following different test liquids (volume of 1×10^{-6} dm^3) were applied: double-distilled water, formamide, and diiodomethane.

The mean value of contact angle, θ, for each test liquid was obtained on the basis of five measurements taken after 5 s of stabilization at different locations on the substrates' surfaces.

XPS spectra were recorded in an ultrahigh vacuum (UHV) chamber (pressure in the 10^{-7}–10^{-6} Pa range) of a SPECS system with a Phoibos MCD 100 electron analyzer and monochromatized Al Kλ X-rays of 1486.7 eV. For the pass energy of 10 eV, the total energy resolution was around 0.8 eV. The photoemission spectra were simulated with several sets of mixed Gaussian-Lorentzian functions with interactive Shirley background subtraction.

The FTIR spectra were recorded on a PerkinElmer Spectrum One FTIR spectrometer (Perkin-Elmer, Waltham, MA, USA). FTIR spectrograms (average of 4 scans) were recorded using the HATR (horizontal attenuated total reflectance) method in the 4000–650 cm^{-1} region with a scan resolution of 4 cm^{-1}. In order to determine the chemical composition and confirm the presence of nickel on the surface of the magnesium AZ91D alloy, XRF (X-ray fluorescence) analysis was performed.

In addition, XRF analysis was performed on a plate of pure magnesium and on a plate of pure nickel. A portable XRF device (Thermo Fisher Scientific Niton XL3t XRF Analyzer, that contains the X-ray tube (the source of X-ray) and Si-PIN detector, all from Thermo Fisher Scientific, Waltham, MA, USA, were used. The X-ray tube is a golden anode with a current intensity operating range of 0–40 μA and excitation potential range of 0–50 kV. The device is factory-calibrated. The unmodified and modified AZ91D magnesium alloy samples were analyzed by standard analysis of thin samples.

3. Results and Discussion

3.1. Chemical Deposition of Nickel

Methods of chemical deposition of nickel are widely used due to the formation of a deposit that uniformly covers the surface of the metal sample and has an extremely high corrosion resistance. Because of the unique chemical reactivity of magnesium alloys, the key to the chemical deposition of highly resistant film of nickel lies in the pretreatment of the alloys.

Since the AZ91D alloy has aluminum content of about 7%, on the surface of the alloy, a chemically deposited Ni film will have poor adhesion properties if the pretreatment process includes pretreatment with a solution of zinc ions. Therefore, new pretreatment procedures for the AZ91D alloy that involve conversion coating with environmentally friendly organic molecules must be developed. According to

Shartal and Kipouros [26], in order to reduce the possibility of galvanic corrosion due to cracking of the porous layer [27], the formed pretreatment film of organic molecules must be sealed.

SAM of DDPA was proposed as a pretreatment layer between the Ni–P layer and AZ91D magnesium alloy samples. Since the surface of the alloy is still porous, the alkylphosphonic acid pretreatment layer needs to be sealed with an alcoholic solution of γ-aminopropyltriethoxysilane (APTES), to which palladium chloride is added.

On thus prepared electrode surface, nickel film was chemically deposited from the bath, which, along with stabilizers, contains nickel acetate as a source of nickel and sodium hypophosphite (H_2PO_2Na) as a reducing agent. For the chemical deposition of nickel, commercial baths that contain hypophosphite are the most commonly used because the hypophosphite increases the deposition rate, stability, and ease of handling the bath.

Although the reactions occurring during the chemical deposition processes have not been completely clarified, the most widely accepted mechanism is that the hypophosphite reduces Pd (II) cations adsorbed onto the surface to the Pd atoms. Pd atoms then catalyze the dehydrogenation of the hypophosphite radicals.

During the dehydrogenation of the hypophosphite radicals, active hydrogen atoms are extracted. The active hydrogen atoms reduce the nickel (II) cations to nickel atoms, which catalyze the dehydrogenation of hypophosphite radicals. Reduced nickel atoms become the activation sites for the precipitation and the nucleation because the autocatalytic nickel deposition reaction is initiated by the catalytic hydrogenation of the reducing agent. Simultaneously, some of the active hydrogen atoms reduce the hypophosphite radical, during which extracts phosphorus. The reactions that occur on the surface of the electrode during the chemical deposition are [8,28]:

$$H_2PO_2^- + H_2O \xrightarrow{\text{catalyst+heating}} H^+ + HPO_3^{2-} + 2H_{abs} \quad (1)$$

$$Ni^{2+} + 2H_{abs} \rightarrow Ni + 2H^+ \quad (2)$$

$$H_2PO_2^- + H_{abs} \rightarrow H_2O + OH^- + P \quad (3)$$

3.1.1. Optimization of the Pretreatment Parameters for the Formation of the Dodecylphosphonic Acid Coating

By the method of electrochemical impedance spectroscopy, optimal parameters for the DDPA ($C_{12}H_{27}PO_3$) SAM formation were determined, since DDPA SAM was proposed as a pretreatment layer between the Ni–P layer and magnesium AZ91D alloy. The experimental parameters that were optimized are the concentration of the DDPA alcohol solution (from 0.5 mmol·dm^{-3} to 10 mmol·dm^{-3}) and the self-assembling time (from 1 h to 4 h).

Figure 1 shows the Nyquist and Bode EIS plots recorded on an AZ91D alloy samples modified with DDPA SAM in the chloride electrolyte solution at the open-circuit potential. DDPA SAM was formed from the alcoholic solution of DDPA by an immersion method. The concentration of DDPA was between 0.5 mmol·dm^{-3} and 10.0 mmol·dm^{-3} and the self-assembling time was 1 h. The Nyquist diagram exhibited two overlapping semicircles. For $\omega \rightarrow 0$, impedance curves in the Nyquist diagram intersecting the real axis, i.e., at Bode diagram plateaus intersect the logarithm of the absolute value of the impedance at the point corresponding to the polarization resistance (R_p). In the medium frequency region of the Bode plots, a linear log$Z$ versus log$f$ dependence and the maximum phase angle on the phase angle, θ, versus log$f$ plots are observed, indicating capacitive behavior of the electrodes. In the Bode plots, the dependence of the phase angle, θ, versus log$f$ also indicates the existence of two time constants. The electric equivalent circuit (EEC) used to fit the experimental data is shown in the inset of Figure 1. The EEC with two time constants is often used to describe the impedance data obtained on the surface of magnesium alloy covered with a film [29–31]. The meanings of the EEC elements are as follows: R_{el} is the electrolyte resistance, R_1–CPE_1 combination represents the outer part of the surface film (i.e., the interfacial film/solution boundary), R_1 is the charge transfer resistance within

the pores of the interfacial oxide/electrolyte boundary, and CPE_1 is the constant phase element that represents a surface capacity of pores of the film. R_2–CPE_2 combination represents the inner part of the surface of the film, that is, its resistance and capacitance.

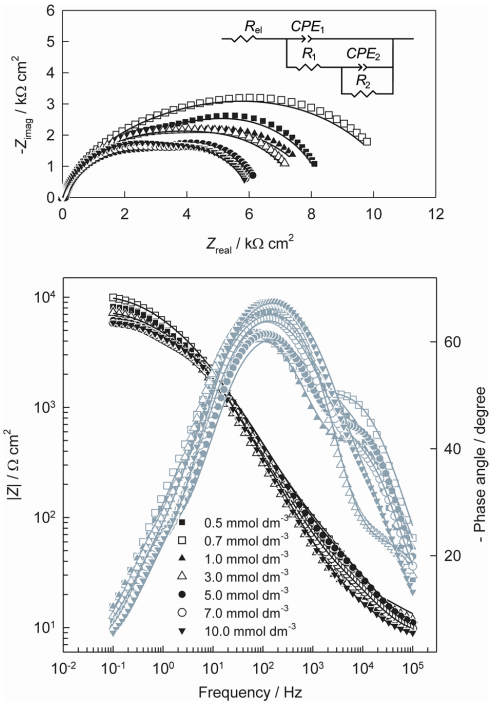

Figure 1. Nyquist and Bode plots for the impedance data of the AZ91D alloy modified with dodecylphosphonic acid (DDPA) self-assembled monolayers (SAMs) recorded in the chloride electrolyte solution at an open-circuit potential (E_{OCP}). Symbols: experimental, solid line: fitting. DDPA SAM was formed from the alcoholic solutions of DDPA at different concentrations. Self-assembling time was 1 h. The inset shows the electric equivalent circuit (EEC) used to fit the impedance spectra.

The presentation of the impedance responses of real dielectric films generally uses constant phase element, CPE. Impedance CPE is described by the expression [32]:

$$Z_{CPE} = [Q(j\omega)^n]^{-1} \quad (4)$$

where the coefficient Q is a combination of properties associated with the state of the surfaces and the electroactive species. j is imaginary number and the exponent n can have values between 1 and -1. For a specific value of n, Equation (4) describes the resistance ($n = 0$), capacity ($n = 1$), inductance ($n = -1$), and the Warburg impedance ($n = 0.5$).

The greatest value of polarization resistance (i.e., the best protective properties) shows AZ91D alloy modified with the DDPA SAM formed in the alcoholic solution with a concentration of 0.7 mmol·dm^{-3}. The reason that poorer protection for the AZ91D alloy samples results from SAMs formed from the alcoholic solution concentration with c(DDPA) > 0.7 mmol·dm^{-3} may be a rapid adsorption rate of DDPA molecules, which results in the formation of less ordered SAMs with a high density of defects [33]. Therefore, a DDPA concentration of c(DDPA) = 0.7 mmol·dm^{-3} is selected for further optimization of the self-assembling time.

The effect of the immersion time on the EIS spectra of the magnesium AZ91D alloy modified with alcoholic solution of DDPA (c = 0.7 mmol·dm^{-3}) is presented in Figure 2. Impedance response in the Nyquist plot is also characterized with two overlapping capacitive semicircles. Higher polarization resistance was obtained when immersion time was 1 h. Extending the immersion time at this concentration of DDPA decreases the polarization resistance of the electrode, which indicates weak

protective properties of the resulting phosphonate SAMs (Figure 2). This can be attributed to the process of accelerated melting of the spontaneously formed oxide film and the creation of defects in the structure of the film that allow direct contact of the magnesium with the ions from the electrolyte solution.

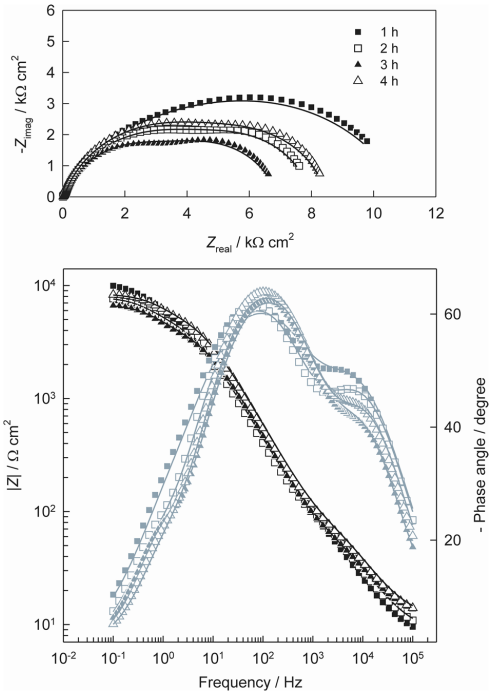

Figure 2. Nyquist and Bode plots for the impedance data of the AZ91D alloy modified with DDPA SAMs recorded in the chloride electrolyte solution at E_{OCP}. Symbols: experimental, solid line: fitting. DDPA SAM was formed from the DDPA alcoholic solutions of 0.7 mmol·dm^{-3} concentration with denoted self-assembling time.

From the impedance response showed in Figures 1 and 2, it is clear that the optimal parameters for obtaining the most corrosion-resistant DDPA pretreatment layer in chloride electrolyte solution are a DDPA solution concentration of 0.7 mmol·dm^{-3} and self-assembling time of 1 h.

Surface characteristics of the DDPA SAMs were investigated using Fourier-transform infrared spectroscopy (FTIR), X-ray photoelectron spectroscopy (XPS), and goniometry (contact angle measurements (CAM)) (Figure 3).

The data in Figure 3A illustrate an XPS spectrum recorded on an AZ91D alloy sample modified with DDPA SAM. The high-resolution spectra of carbon, oxygen, and phosphorus were deconvoluted using component peaks in order to determine the possible bonding modes of the DDPA molecules with the oxide layer on the alloy surface. The C 1s electrons emission peak was deconvoluted into three Voight curves with binding energies (BE) of 285.0 eV, 285.8 eV, and 289.0 eV, which can be attributed to the alkyl chain (C–C, C–H), the carbon bonded to phosphorus, and surface impurities [34,35]. The peak attributed to the alkyl chain (C–C, C–H) and a peak attributed to the carbon bonded to phosphorus indicates that the surface coverage of DDPA molecules could be high [34]. The fitting of a P 2p peak was conducted with two doublets, $2p_{1/2}$ and $2p_{3/2}$ components of the energy splitting of 0.88 eV, and intensity ratio of 0.5. The first doublet of 131.1 eV is attributed to the metal bonded to phosphonate oxygen (P–O–M) [36], and the second, at 133.7 eV, is attributed to the O=P–OH group bonded to the metal surface [36,37]. The O 1s emission peaks were deconvoluted using four Voight curves with BEs of 530.9 eV, 531.8 eV, 532.9 eV, and 533.9 eV, which can be attributed to the oxide ions (O^{2-}), mainly MgO [34,38,39], phosphonate oxygen bonded to the metal (P–O–M) [30,37–41], P–OH group [38–40,42], and P=O group [39,40]. A dominant peak attributed to phosphonate oxygen bonded

to the metal (P–O–M) [30,37–41] has been attributed to metallic hydroxide by Ishizaki et al., and a few other authors have attributed it to the P=O bond [30,37,39,41] as well as phosphonate oxygen-metal bond. The presence of P–OH groups can contribute to cross-link stabilization of the SAM by allowing hydrogen bond interactions between adhesive groups. The oxygen O 1s data and the phosphorous P 2p data indicate that the DDPA molecules are bonded covalently to the oxidized magnesium AZ91D alloy surface. The presence of the peaks attributed to P–O–M, P=O, and P–OH bonds indicates that in the phosphonate SAMs formed at the metal surface, alkylphosphonic acids can be mono-, bi- and tridentate bonded. The data obtained are in good agreement with those for SAM of *n*-octylphosphonic acid bonded to AZ31 magnesium alloy reported by Ishizaki and colleagues [30,43].

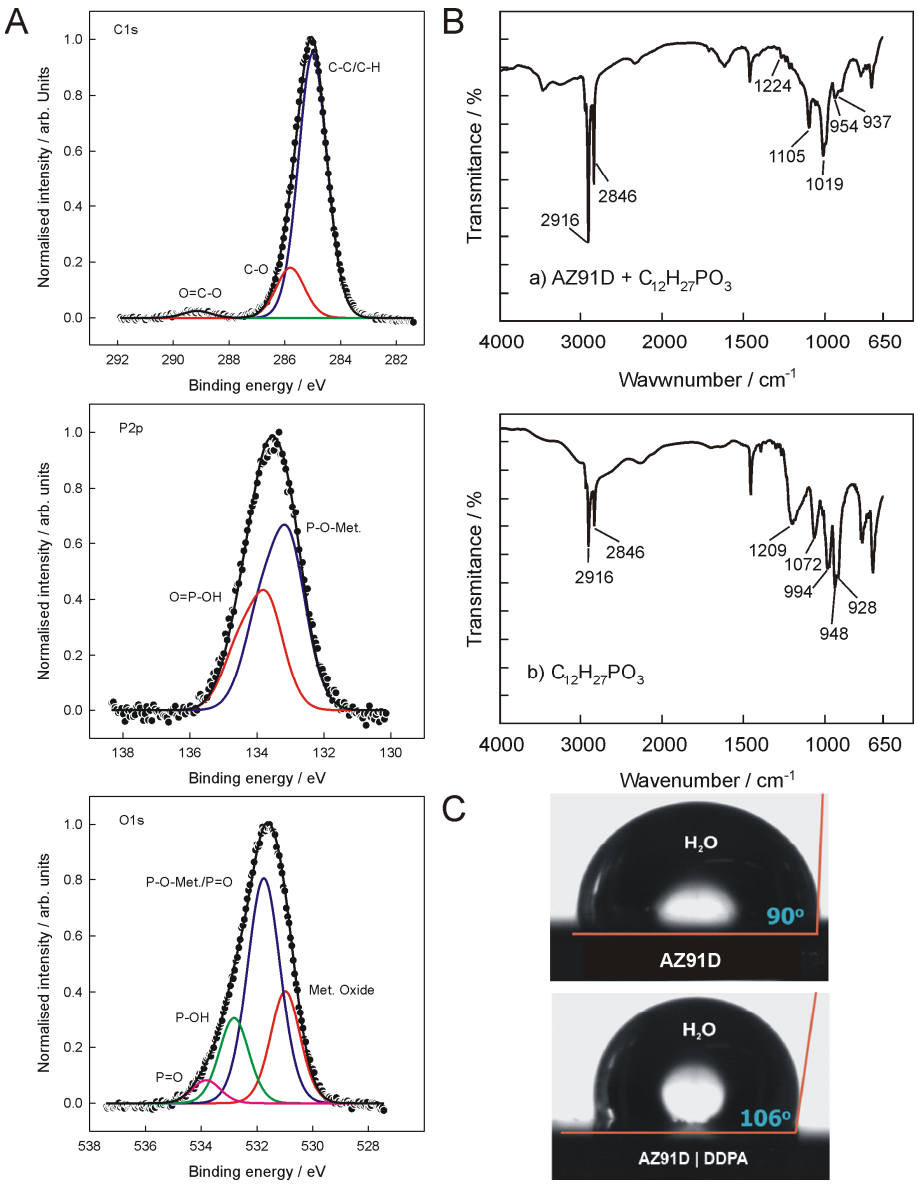

Figure 3. (**A**) The deconvoluted X-ray photoelectron spectroscopy (XPS) spectra of C 1s, P 2p, and O 1s electrons obtained for AZ91D alloy modified with DDPA SAM; (**B**) Fourier-transform infrared spectroscopy (FTIR) spectra of DDPA SAM-modified AZ91D alloy (**a**) and DDPA powder (**b**); (**C**) optical micrographs of a water drop on unmodified AZ91D alloy and on AZ91D alloy modified with DDPA SAM. [43]

The FTIR spectra of AZ91D alloy on which DDPA SAMs are formed and FTIR spectra of DDPA powder were recorded and are shown in Figure 3B. Both spectra contain peaks at 2916.5 cm^{-1} and 2845.6 cm^{-1}, which can be attributed to the asymmetric (2916.5 cm^{-1}) and symmetric (2845.6 cm^{-1}) C–H stretching of methylene group (–CH_2). As an FTIR spectra containing $\upsilon(CH_2)_{asymm.} \leq 2918$ cm^{-1} and $\upsilon(CH_2)_{symm.} \leq 2848$ cm^{-1} is characteristic of a well-ordered monolayer [37,44–46], it can be concluded that on the surface of AZ91D alloy, the formed DDPA SAMs are well arranged. The PO region of the DDPA powder contains a broad peak at 1208.7 cm^{-1} attributed to the stretching vibration of P=O bond, peaks at 1072.2 cm^{-1} and 993.8 cm^{-1} attributed to the stretching vibration of P–O bond, and peaks at 948.3 cm^{-1} and 928.1 cm^{-1} attributed to the stretching vibration of P–OH bond. The PO region of the AZ91D alloy, on whose surface DDPA SAM was formed, is shifted to a higher frequency range and contains peaks at 1105.1 cm^{-1} and 1019.1 cm^{-1} that can be attributed to the stretching vibration of the P–O bond, which indicates that the phosphonic acid is on the oxidized AZ91D alloy surface, bonded through head groups.

However, the FTIR spectrum of AZ91D alloy with DDPA SAM contains peaks of weak intensity at 954 cm^{-1} and 937 cm^{-1} (corresponding to stretching vibration of the P–OH bond) and a peak of weak intensity around 1224 cm^{-1} (corresponding to stretching vibration of the P=O bond), which suggest the presence of a number of different binding modes in DDPA monolayers. Two broad bands in the FTIR spectrum of DDPA powder of weak to medium-strong intensity at 2700–2500 cm^{-1} and 2300–2100 cm^{-1} are because of the O–H stretching characteristic for compounds which contain a P–OH group [47,48]. The peak of low intensity in the FTIR spectrum of AZ91D alloy with DDPA SAM at a wavenumber of about 2300 cm^{-1} confirms the presence of free P–OH groups in DDPA SAM.

The data in Figure 3C illustrate the contact angles of a drop of water close to the surface of unmodified AZ91D alloy surface and the surface of AZ91D alloy modified with DDPA SAM. The water contact angles measured on the AZ91D alloy modified with phosphonate SAM indicate a high hydrophobicity of the formed SAM, which is the result of several factors, including the well-ordered and densely packed monolayers, the hydrophobic terminal methyl group oriented outward, and a van der Waals interaction between alkyl chains. The water contact angle of DDPA on the magnesium AZ91D alloy (106°) is almost identical to that of DDPA (105°) on the magnesium AZ31 alloy [36].

3.1.2. Modification of Alkylphosphonic Acid Pretreatment Film with APTES

Optimized DDPA SAM on AZ91D alloy was the starting point for the further modification with APTES. First step in the application of APTES is hydrolysis of the APTES, thus obtaining γ-aminopropyltrihydroxysilane (APTHS) with capability of forming of Si–OH groups (see Figure 4). APTHS is then chemically adsorbed through hydrogen bonding at the surface of the alloy enriched with OH groups that originate from the DDPA SAM pretreatment film. In a second step, dissolving of $PdCl_2$ in the APTHS solution results in a substitution reaction (S_N2 mechanism) and production of the Pd (II) complex occurs; water and/or chloride ions are substituted with an amino group (NH_2) of APTHS. The resulting coordinative covalent bond of the Pd(II)–APTHS ($Pd(II)NH_2(CH_2)_3Si(OH)_3$) complex is extremely strong. This arises from the fact that the amino group is the strong electron donor, thus forming coordinate covalent bonds where a free electron pair of amino groups will fill an empty dsp^2 hybrid orbital of Pd^{2+} ions of sufficiently low energy [8]. The condensation reaction of the DDPA SAM pretreatment film and the Pd(II)–APTHS complex is shown in Figure 4A and the FTIR spectrum confirming this reaction is shown in Figure 4B.

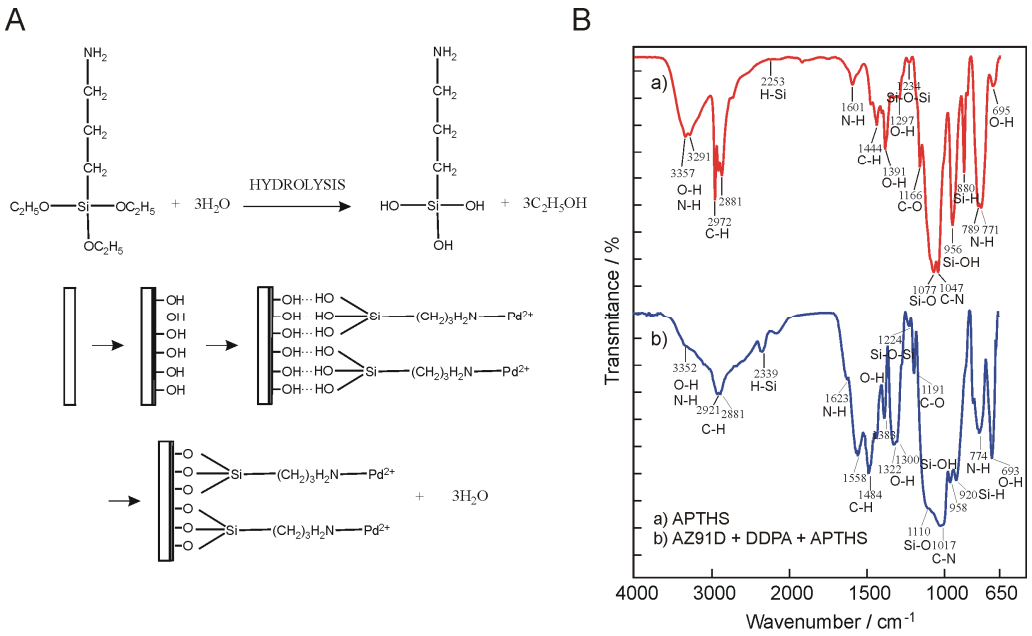

Figure 4. (**A**). The condensation scheme of the DDPA SAM pretreatment film with the Pd(II)–γ-aminopropyltrihydroxysilane (APTHS, $H_2N(CH_2)_3Si(OH)_3$) complex; (**B**) FTIR spectra of APTHS (**red**) and modified AZ91D magnesium alloy on which DDPA SAM pretreatment film is sealed with APTHS (**blue**).

When comparing FTIR spectra of the AZ91D alloy surface (modified with DDPA SAM and APTHS) and pure APTHS, peaks at very similar wavenumbers (Figure 4A) can be observed. In addition, peak shifts to higher wavenumbers (in the case of modified AZ91D alloy) compared to the pure APTHS can be observed. This indicates the chemical reaction between the Si–OH group of APTHS and a hydroxyl group of DDPA, whose products can be absorbed on the alloy surface. Amplification of the peaks' intensity as well as "deformation" of some peaks in the FTIR spectra (in the case of the alloy surface) can be explained by overlapping APTHS peaks with those of DDPA in the area of wavenumbers from 1200–950 cm^{-1} attributed to P–O stretching [47,48]. From obtained FTIR spectra it can be concluded presence of DDPA SAM and APTHS on the surface layer.

3.1.3. The Modification of the Pretreatment Film by Ni–P Coating

On the above-prepared surface, chemical deposition of the nickel film was performed. After the film of nickel was formed, its corrosion stability was examined by EIS. Figure 5 shows the effect of bath temperature (A) and the time of deposition (at constant temperature of 70 °C (B)) on the impedance spectra of the AZ91D alloy on which the film of nickel was chemically deposited; the spectra were recorded after 30 min of stabilization in the chloride electrolyte solution at an open-circuit potential. As can be seen in Figure 5A, an increase of the electrode polarization resistance is obtained when reducing the temperature of the bath from 85 °C to 70 °C. At the constant temperature of 70 °C, the highest polarization resistance was obtained when deposition time was 60 s (Figure 5B). When bath temperature is lower than 70 °C and there is a prolonged deposition time (longer than 60 s), polarization resistance decreases. For comparison, the impedance spectra of pure nickel, recorded at the same conditions, is presented (inset of Figure 5A). As can be seen, the Nyquist plot shows a capacitive semicircle which is not "closed", and which crosses the straight line at an angle of 45°, indicating the presence of the Warburg impedance characteristic for the process of diffusion [49].

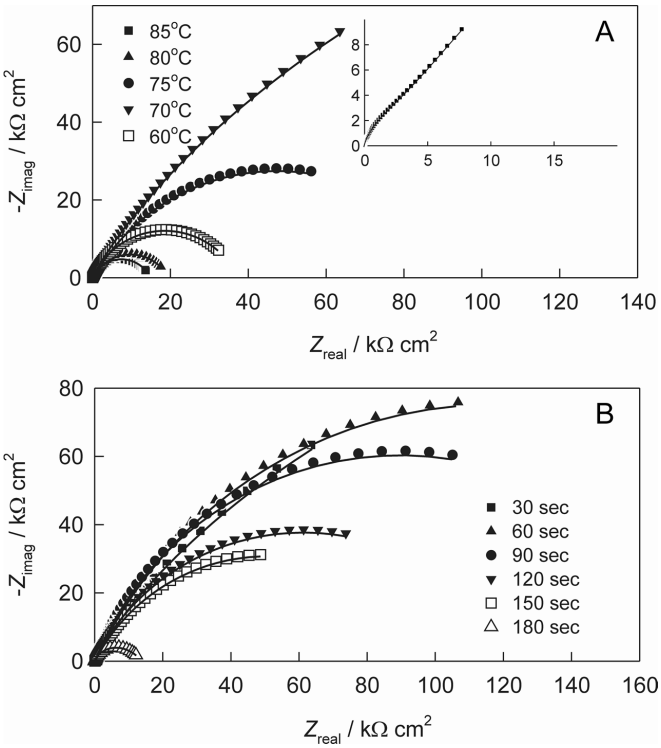

Figure 5. Electrochemical impedance spectra of AZ91D alloy modified with chemically deposited film of nickel recorded in the chloride electrolyte solution at the open-circuit potential; (**A**) optimization of the bath temperature (at constant deposition time of 30 s); and (**B**) optimization of the deposition time (at constant temperature of 70 °C). Symbols: experimental, solid line: fitting. The inset of (**A**) is the impedance spectra of the electrode of pure nickel recorded in chloride electrolyte solution at the open-circuit potential. Symbols: experimental, solid line: fitting.

3.2. Electrochemical Deposition of Nickel

Nickel was electrodeposited from a commercial Watt bath with temperature of 40 °C at −5.88 mA for 5 min. The electrochemical impedance spectroscopy method was used to examine the corrosion resistance of AZ91D alloy modified with an electrodeposited film of nickel. The spectra were recorded in the chloride electrolyte solution on the open-circuit potential after 30 min of stabilization. The shape of the spectrum (not shown here) is identical to that shown in Figure 1, and mathematically modeled using the same EEC. The values of polarization resistance (R_p) and film capacitance values (CPE_2)—which represents the film capacitance as a function of the nickel deposition process—are presented in Figure 6. From the figure, it is evident that the electrodes of AZ91D alloy, pretreated and modified with chemically deposited nickel film, have a higher polarization resistance (R_p = 533 kΩ·cm^2) (i.e., are more resistant to corrosion) in chloride electrolyte solution than the electrodes modified with electrochemically deposited nickel film (R_p = 475 kΩ·cm^2). The CPE_2 of the AZ91D alloy samples are 7.51 × 10^{-6} Ω^{-1}·cm^{-2}·s^n for the AZ91D | Ni (chemically deposited) and 9.53 × 10^{-6} Ω^{-1}·cm^{-2}·s^n for the AZ91D | Ni (electrochemically deposited) (Figure 6). From the values of the CPE_2 element, it can be concluded that the nickel film deposited chemically (from the bath with temperature of 70 °C and for a duration of 60 s) is thicker and less porous.

Coverage, θ, of the AZ91D surface by film of nickel is calculated according to the expression:

$$\theta = (R_{p(AZ91D|Ni)} - R_{p(AZ91D)})/R_{p(AZ91D|Ni)} \quad (5)$$

$R_{p(AZ91D)}$ and $R_{p(AZ91D|Ni)}$ are the polarization resistance values of AZ91D alloy coated with spontaneously formed oxide film (4 kΩ·cm^2) and nickel film, respectively. The coverage of nickel film formed chemically as well as the coverage formed electrochemically are 99%.

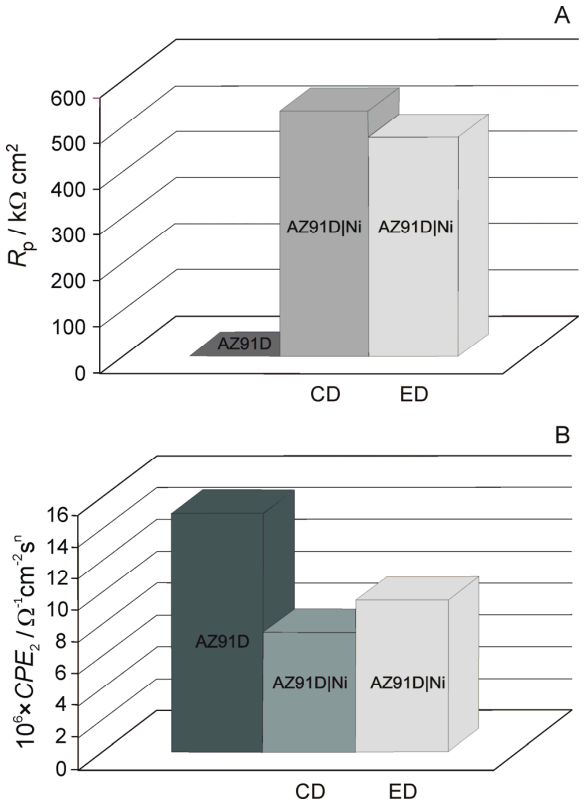

Figure 6. (**A**) The values of polarization resistance (R_p) and (**B**) the values of film capacitance (CPE_2) as a function of the nickel deposition process using chemical deposition (CD) and electrochemical deposition (ED). Chemical deposition was carried out with the b ath temperature of 70 °C for 60 s and electrodeposition was carried out from the bath temperature of 40 °C at −5.88 mA for 5 min.

In our work, the corrosion protection enhancement is equivalent (99%) to that of the Ni–P coating of Cui et al. [8], who have reported that Ni–P coating can be plated on the AZ91D alloy coated with phytic acid conversion coatings. Additionally, in our work, the nickel film—formed chemically as well as formed electrochemically—gives better corrosion protection (higher polarization resistance) for the AZ91D alloy than the one for the magnesium alloys chemically treated in an aqueous solution of $Ce(NO_3)_3$, $ZrO(NO_3)_2$, and $Nb_xO_yF_z$ reported by Ardelean et al. [50]. Polarization resistance for the Ce–Zr–Nb-treated magnesium alloys is higher than that for the similar DOW22-treated Mg alloys (Cr^{6+}-based coatings, 15 w/v% $Na_2Cr_2O_7 \times 2H_2O$ + 0.5 w/v% $KMnO_4$ + 0.25 v/v% H_2SO_4 in water), while the DOW22 treatment leads to an almost identical corrosion resistance as that for the untreated alloy [50].

XRF analysis was used to verify existence of the nickel film on the surface of AZ91D alloy. The composition of the surface layer of AZ91D alloy samples is illustrated in Table 1 and Figure 7. Modification of the alloy surface with the film of nickel was conducted by chemical deposition (from the bath temperature of 70 °C for 60 s) and electrochemical deposition (from the Watts bath temperature of 40 °C at −5.88 mA for 5 min). Since the device for XRF analysis lacked a plug required for the determination of magnesium for comparison and XRF analysis of plates of magnesium was performed. Analysis has shown that the sample contains even 99.937% of aluminum, however, the given percentage is the weight percentage of aluminum in the sample, from which it can be concluded that with magnesium, the next the most abundant element in the sample is aluminum.

As it can be seen, the results of the XRF analysis confirm the existence of nickel film on the AZ91D alloy surface.

Table 1. The mass percentages of the elements obtained from the results of X-ray fluorescence (XRF) analysis for the unmodified AZ91D alloy sample and AZ91D alloy sample modified with the nickel film.

Alloy	Pd	Al	Pb	Zn	Cu	Ni	Fe	Mn	Cr	V	Ti
AZ91D	LOD	99.036	LOD	0.704	LOD	LOD	LOD	0.224	LOD	0.028	LOD
AZ91D | Ni (CD)	0.051	98.784	LOD	0.465	LOD	0.621	LOD	0.057	LOD	0.008	LOD
AZ91D | Ni (ED)	LOD	99.318	0.002	0.133	LOD	0.490	LOD	0.027	LOD	0.008	0.013

Note: CD—chemical deposition; ED—electrochemical deposition; LOD—below the limit of detection.

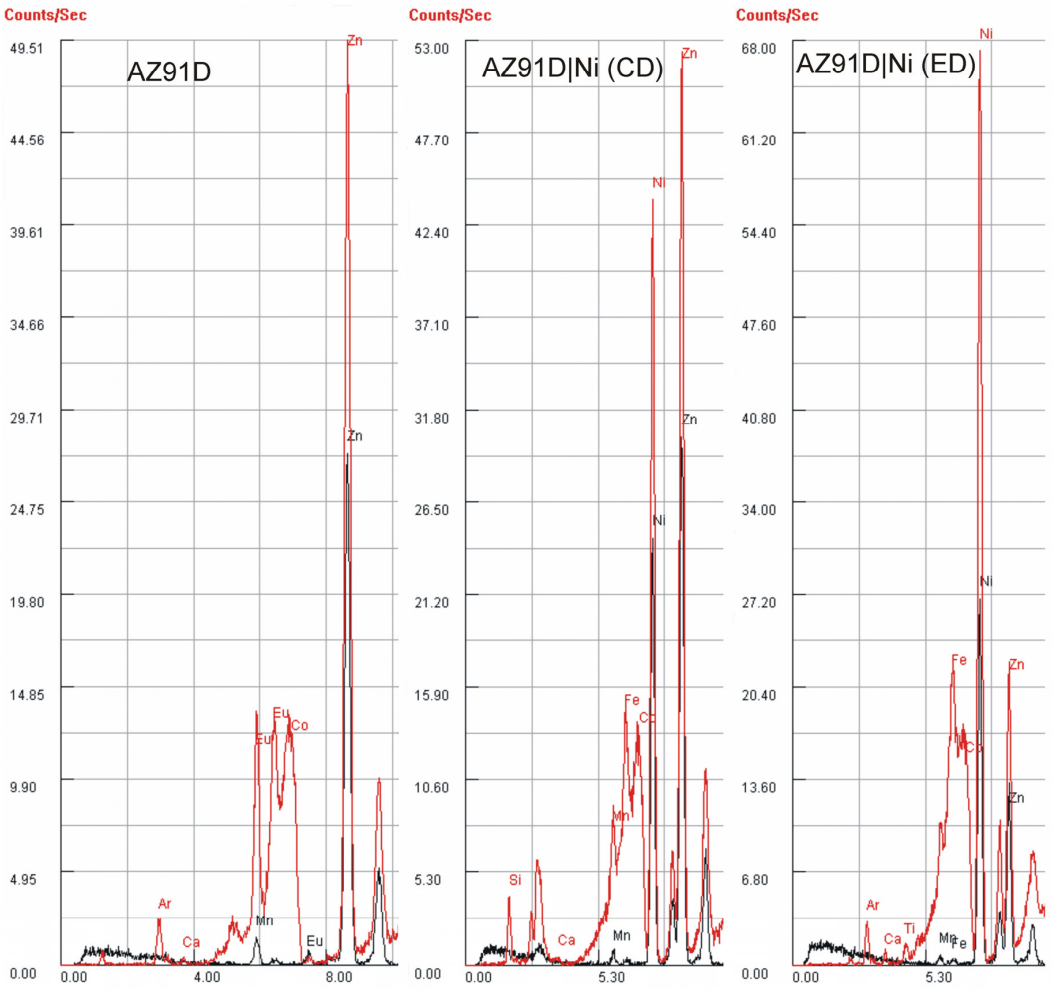

Figure 7. The spectra obtained by XRF analysis of unmodified AZ91D alloy sample and AZ91D alloy sample modified with nickel film formed by chemical or electrochemical deposition.

4. Conclusions

In this work, we presented environmentally friendly surface modification of the AZ91D Mg alloy with alkylphosphonic acid followed by sealing with γ-aminopropyltriethoxysilane (APTES) in order to obtain a quality surface for chemical deposition of nickel.

The polarization resistances, obtained by EIS, suggest that the best characteristics (electrochemical and physical) of the self-assembled monolayer (SAM) of dodecylphosphonic acid (DDPA) can be obtained during immersion of alloy in 0.7 mmol·dm^{-3} solution of DPPA for 1 h. Data obtained by

XPS suggest that the formed SAM can be mono-, bi-, and tridentate bonded. This is also proven by FTIR analysis.

On the DPPA SAM layer, deposition of APTHS by adsorption, followed by formation of a Pd (II) complex, was successfully performed.

Optimization of the procedure for chemical deposition of nickel, on the above-prepared layer, revealed that the best layer was obtained at 70 °C for 60 s.

Values of the EEC elements derived from EIS spectra revealed that the nickel film deposited chemically (from the bath temperature of 70 °C for 60 s) is thicker, less porous, and has higher polarization resistance than the layer obtained electrochemically.

The results presented in this work suggest that pretreatment of AZ91D alloy with an environmentally friendly conversion layer, based on DPPA and APTHS, has great and promising potential for application and utilization.

Acknowledgments: This publication would not have been possible without the generous support of Zoran Grubač and Marijo Buzuk.

Author Contributions: Ivana Škugor Rončević wrote the original manuscript and conceived experiments. Mirjana Metikoš-Huković supervised experimental work, revised the manuscript and suggested improvements of manuscript. Marijo Buzuk and Nives Vladislavić performed the experiments, analyzed the data and helped wrote the manuscript.

Conflicts of Interest: The authors declare no conflict of interest.

References

1. Zeng, L.; Yang, S.; Zhang, W.; Guo, Y.; Yan, C. Preparation and characterization of a double-layer coating on magnesium alloy AZ91D. *Electrochim. Acta* **2010**, *55*, 3376–3383. [CrossRef]
2. Gray, J.E.; Luan, B. Protective coatings on magnesium and its alloys—A critical review. *J. Alloy. Compd.* **2002**, *336*, 88–113. [CrossRef]
3. Song, Y.W.; Shan, D.Y.; Han, E.H. High corrosion resistance of electroless composite plating coating on AZ91D magnesium alloys. *Electrochim. Acta* **2008**, *55*, 2135–2143. [CrossRef]
4. Gu, C.; Lian, J.; Li, G.; Niu, L.; Jiang, Z. Electroless Ni–P plating on AZ91D magnesium alloy from a sulfate solution. *J. Alloy. Compd.* **2005**, *391*, 105–109. [CrossRef]
5. Mahallawy, N.E.; Bakkar, A.; Shoeib, M.; Palkowski, H.; Neubert, V. Electroless Ni-P coating of different magnesium alloys. *Surf. Coat. Technol.* **2008**, *202*, 5151–5157. [CrossRef]
6. Aal, A.A. Protective coating for magnesium alloy. *J. Mater. Sci.* **2008**, *43*, 2947–2954.
7. Song, G.; Atrens, A. Corrosion mechanisms of magnesium alloys. *Adv. Eng. Mater.* **1999**, *1*, 11–33. [CrossRef]
8. Cui, X.; Jin, G.; Li, Q.; Yang, Y.; Li, Y.; Wang, F. Electroless Ni-P plating with a phytic acid pretreatment on AZ91D magnesium alloy. *Mater. Chem. Phys.* **2010**, *121*, 308–313. [CrossRef]
9. Yang, H.Y.; Chen, X.B.; Guo, X.W.; Wu, G.H.; Ding, W.J.; Birbilis, N. Coating pretreatment for Mg alloy AZ91D. *Appl. Surf. Sci.* **2012**, *258*, 5472–5481. [CrossRef]
10. Chen, X.B.; Birbilis, N.; Abbott, T.B. Review of Corrosion-Resistant Conversion Coatings for Magnesium and Its Alloys. *Corrosion* **2011**, *67*, 035005-1–035005-16. [CrossRef]
11. Chiu, K.Y.; Wong, M.H.; Cheng, F.T.; Man, H.C. Characterization and corrosion studies of fluoride conversion coating on degradable Mg implants. *Surf. Coat. Technol.* **2007**, *202*, 590–598. [CrossRef]
12. Yang, K.H.; Ger, M.D.; Hwu, W.H.; Sung, Y.; Liu, Y.C. Study of vanadium-based chemical conversion coating on the corrosion resistance of magnesium alloy. *Mater. Chem. Phys.* **2007**, *101*, 480–485. [CrossRef]
13. Chen, X.-B.; Birbilis, N.; Abbott, T.B. Effect of [Ca^{2+}] and [PO_4^{3-}] levels on the formation of calcium phosphate conversion coatings on die-cast magnesium alloy AZ91D. *Corros. Sci.* **2012**, *55*, 226–232. [CrossRef]
14. Huo, H.; Li, Y.; Wang, F. Corrosion of AZ91D magnesium alloy with a chemical conversion coating and electroless nickel layer. *Corros. Sci.* **2004**, *46*, 1467–1477. [CrossRef]
15. Zucchi, F.; Frignani, A.; Grassi, V.; Trabanelli, G.; Monticelli, C. Stannate and permanganate conversion coatings on AZ31 magnesium alloy. *Corros. Sci.* **2007**, *49*, 4542–4552. [CrossRef]
16. Wang, C.; Zhu, S.; Jiang, F.; Wang, F. Cerium conversion coatings for AZ91D magnesium alloy in ethanol solution and its corrosion resistance. *Corros. Sci.* **2009**, *51*, 2916–2923. [CrossRef]

17. Birbilis, N.; Howlett, P.C.; MacFarlane, D.R.; Forsyth, M. Exploring corrosion protection of Mg via ionic liquid pretreatment. *Surf. Coat. Technol.* **2007**, *201*, 4496–4504. [CrossRef]
18. Song, Y.; Shan, D.; Chen, R.; Zhang, F.; Han, E.-H. A novel phosphate conversion film on Mg-8.8Li alloy. *Surf. Coat. Technol.* **2009**, *203*, 1107–1113. [CrossRef]
19. He, M.; Liu, L.; Wu, Y.; Tang, Z.; Hu, W. Corrosion properties of surface-modified AZ91D magnesium alloy. *Corros. Sci.* **2008**, *50*, 3267–3273.
20. Ng, W.F.; Wong, M.H.; Cheng, F.T. Stearic acid coating on magnesium for enhancing corrosion resistance in Hanks' solution. *Surf. Coat. Technol.* **2010**, *204*, 1823–1830. [CrossRef]
21. Radošević, J. Ekološki prihvatljivi inhibitori korozije legura aluminija i bakra. *Zaštita Mater.* **2012**, *53*, 313–323.
22. Zhao, M.; Wu, S.; Luo, J.; Fukuda, Y.; Nakae, H. A chromium-free conversion coating of magnesium alloy by a phosphate-permanganate solution. *Surf. Coat. Technol.* **2006**, *200*, 5407–5412. [CrossRef]
23. Anık, M.; Körpe, E. Effect of alloy microstructure on electroless NiP deposition behavior on Alloy AZ91. *Surf. Coat. Technol.* **2007**, *201*, 4702–4710. [CrossRef]
24. Chong, K.Z.; Shih, T.S. Conversion-coating treatment for magnesium alloys by a permanganate-phosphate solution. *Mater. Chem. Phys.* **2003**, *80*, 191–200. [CrossRef]
25. Elsentriecy, H.H.; Azumi, K. Electroless Ni-P deposition on AZ91 D agnesium alloy prepared by molybdate chemical conversion coatings. *J. Electrochem. Soc.* **2009**, *156*, 70–77. [CrossRef]
26. Shartal, K.H.M.; Kipouros, G.J. Electroless nickel phosphorus plating on AZ31. *Metall. Mater. Trans. B* **2009**, *40*, 208–222. [CrossRef]
27. Wu, L.; Zhao, J.; Xie, Y.; Yang, Z. Progress of electroplating and electroless plating on magnesium alloy. *Trans. Nonferr. Met. Soc. China* **2010**, *20*, 630–637. [CrossRef]
28. Sunb, S.; Liu, J.; Yan, C.; Wang, F. A novel process for electroless nickel plating on anodized magnesium alloy. *Appl. Surf. Sci.* **2008**, *254*, 5016–5022.
29. Grubač, Z.; Rončević, I.Š.; Huković, M.M.; Babić, R.; Petravić, M.; Peter, R. Surface Modification of Biodegradable Magnesium Alloys. *J. Electrochem. Soc.* **2012**, *159*, C1–C6. [CrossRef]
30. Ishizaki, T.; Okido, M.; Masuda, Y.; Saito, N.; Sakamoto, M. Corrosion resistant performances of alkanoic and phosphonic acids derived self-assembled monolayers on magnesium alloy AZ31 by vapor-phase method. *Langmuir* **2011**, *27*, 6009–6017. [CrossRef] [PubMed]
31. Zhang, S.; Zhang, X.; Zhao, C.; Li, J.; Song, Y.; Xie, C.; Tao, H.; Zhang, Y.; He, Y.; Jiang, Y.; et al. Research on an Mg-Zn alloy as a degradable biomaterial. *Acta Biomater.* **2010**, *6*, 626–640. [CrossRef] [PubMed]
32. Macdonald, J.R. *Impedance Spectroscopy: Emphasizing Solid Materials and Systems*; John Wiley & Sons: New York, NY, USA, 1987.
33. Liu, J.; Guo, Y.; Huang, W. Study on the corrosion resistance of phytic acid conversion coating for magnesium alloys. *Surf. Coat. Technol.* **2006**, *201*, 1536–1541.
34. Milošev, I.; Huković, M.M.; Petrović, Ž. Influence of preparation methods on the properties of self-assembled films of octadecylphosphonate on NiTi: XPS and EIS studies. *Mater. Sci. Eng. C* **2012**, *32*, 2604–2616. [CrossRef]
35. Liakos, I.L.; McAlpine, E.; Chen, X.; Newman, R.; Alexander, M.R. Assembly of octadecyl phosphonic acid on air annealed alumina. *Appl. Surf. Sci.* **2008**, *255*, 3276–3282. [CrossRef]
36. Ishizaki, T.; Teshima, K.; Masuda, Y.; Sakamoto, M. Liquid phase formation of alkyl- and perfluoro-phosphonic acid derived monolayers on magnesium alloy AZ31 and their chemical properties. *J. Colloid Interface Sci.* **2011**, *360*, 280–288. [CrossRef] [PubMed]
37. Zorn, G.; Gotman, I.; Gutmanas, E.Y.; Adadi, R.; Salitra, G.; Sukenik, C.N. Surface Modification of Ti45Nb Alloy with an Alkylphosphonic Acid Self-Assembled Monolayer. *Chem. Mater.* **2006**, *17*, 4218–4226. [CrossRef]
38. Adolphi, B.; Jähne, E.; Busch, G.; Cai, X. Characterization of the adsorption of ω-(thiophene-3-yl alkyl) phosphonic acid on metal oxides with AR-XPS. *Anal. Bioanal. Chem.* **2004**, *379*, 646–652. [CrossRef] [PubMed]
39. Bhure, R.; Fattah, T.M.A.; Bonner, C.; Hall, F.; Mahapatro, A. Stability of Phosphonic Self Assembled Monolayers (SAMs) on Cobalt Chromium (Co-Cr) Alloy under Oxidative conditions. *Appl. Surf. Sci.* **2011**, *257*, 5605–5612. [CrossRef] [PubMed]
40. Gouzman, I.; Dubey, M.; Carolus, M.D.; Schwartz, J.; Bernasek, S.L. Monolayer vs. multilayer self-assembled alkylphosphonate films: X-ray photoelectron spectroscopy studies. *Surf. Sci.* **2006**, *600*, 773–781. [CrossRef]

41. Hofer, R.; Textor, M.; Spencer, N.D. Alkyl Phosphate Monolayers, Self-Assembled from Aqueous Solution onto Metal Oxide Surfaces. *Langmuir* **2001**, *17*, 4014–4020. [CrossRef]
42. Mani, G.; Johnson, D.M.; Marton, D.; Dougherty, V.L.; Feldman, M.D.; Patel, D.; Ayon, A.A.; Agrawal, C.M. Stability of Self-Assembled Monolayers on Titanium and Gold. *Langmuir* **2008**, *24*, 6774–6784. [CrossRef] [PubMed]
43. Grubač, Z.; Huković, M.M.; Babić, R.; Rončević, I.Š.; Petravić, M.; Peter, R. Functionalization of biodegradable magnesium alloy implants with alkylphosphonate self-assembled films. *Mater. Sci. Eng. C* **2013**, *33*, 2152–2158.
44. Huković, M.M.; Babić, R.; Petrović, Ž.; Posavec, D. Copper Protection by a Self-Assembled Monolayer of Alkanethiol: Comparison with Benzotriazole. *J. Electrochem. Soc.* **2007**, *154*, C138–C143. [CrossRef]
45. Wan, Y.; Wang, Y.; Zhang, Q.; Wang, Z.; Xu, Z.; Liu, C.; Zhang, J. Enhanced tribology durability of a self-assembled monolayer of alkylphosphonic acid on a textured copper substrate. *Appl. Surf. Sci.* **2012**, *259*, 147–152. [CrossRef]
46. Quiñones, R.; Raman, A.; Gawalt, E.S. Functionalization of nickel oxide using alkylphosphonic acid self-assembled monolayers. *Thin Solid Films* **2008**, *516*, 8774–8781. [CrossRef]
47. Maege, I.; Jaehne, E.; Henke, A.; Adler, H.J.P.; Bram, C.; Jung, C.; Stratmann, M. Self-assembling adhesion promoters for corrosion resistant metal polymer interfaces. *Prog. Org. Coat.* **1998**, *34*, 1–12. [CrossRef]
48. Fonder, G.; Minet, I.; Volcke, C.; Devillers, S.; Delhalle, J.; Mekhalif, Z. Anchoring of alkylphosphonic derivatives molecules on copper oxide surfaces. *Appl. Surf. Sci.* **2011**, *257*, 6300–6307. [CrossRef]
49. Cheong, W.-J.; Luan, B.L.; Shoesmith, D.W. Protective coating on Mg AZ91D alloy—The effect of electroless nickel (EN) bath stabilizers on corrosion behaviour of Ni–P deposit. *Corros. Sci.* **2007**, *49*, 1777–1798. [CrossRef]
50. Ardelean, H.; Frateur, I.; Marcus, P. Corrosion protection of magnesium alloys by cerium, zirconium and niobium-based conversion coatings. *Corros. Sci.* **2008**, *50*, 1907–1918. [CrossRef]